Pergamon

Corrosion Science, Vol. 37, No. 2, pp. 211–229, 1995
Copyright © 1995 Elsevier Science Ltd
Printed in Great Britain. All rights reserved
0010–938X/95 $9.50 + 0.00

0010–938X(94)00108–1

A COMPARATIVE STUDY ON THE PASSIVATION AND LOCALIZED CORROSION OF α, β, AND $\alpha + \beta$ BRASS IN BORATE BUFFER SOLUTIONS CONTAINING SODIUM CHLORIDE—I. ELECTROCHEMICAL DATA

J. MORALES,* G. T. FERNANDEZ,* P. ESPARZA,* S. GONZALEZ,* R. C. SALVAREZZA† and A. J. ARVIA†

*Dpto. de Química Física, Universidad de La Laguna, Tenerife, Spain
†INIFTA, Sucursal 4, Casilla de Correo 16, (1900) La Plata, Argentina

Abstract—The passivation and localized corrosion of α-, β-, and $(\alpha + \beta)$-brass in borate–boric acid buffer solutions (pH 9) containing different NaCl concentrations (c_{NaCl}) were studied comparatively using conventional electrochemical techniques at 25°C. The passivation of brass in borate–boric acid buffer was due to the electroformation of a complex passive layer consisting of $ZnO \cdot xH_2O$ and Cu_2O–CuO. In NaCl-containing borate–boric acid buffer the breakdown of the passive layer occurs leading to pitting corrosion when the applied potential exceeds a certain critical value, E_b. For a given type of brass, the value of E_b is shifted negatively as c_{NaCl} is increased. At a constant c_{NaCl} the localized corrosion resistance of brass increases in the following order $(\alpha + \beta)$-brass $\cong$ β-brass $<$ α-brass. For all brass the localized corrosion resistance was lower than that of polycrystalline Cu, but considerably greater than that of polycrystalline Zn. Passive film composition and de-alloying can account for the localized corrosion resistance of these alloys.

INTRODUCTION

The stability of binary alloys such as Cu–Zn alloys (brass) in different aqueous environments has been extensively studied over a wide range of experimental conditions.[1–4] It depends on the alloy composition, the distribution of Cu and Zn oxides and their atomic species at the alloy surface,[5] the solution composition,[6] the surface pretreatment and the temperature.[7]

The Cu–Zn phase diagram indicates the appearance of single and multiphase domains, depending on the Cu/Zn ratio in the alloy and temperature. At room temperature the following stable phases are grown, namely, α-brass phase ($70 < Cu < 100, 0 < Zn < 30$), β-phase ($52 < Cu < 55, 45 < Zn \leq 48$) or the $(\alpha + \beta)$-phase ($55 < Cu < 70, 30 < Zn < 45$).[8]

The study of the corrosion and passivation of brasses has been particularly oriented towards dezincification and stress corrosion cracking of this material in neutral and alkaline solutions.[1–4] Corrosion and passivation of brass have been interpreted in terms of a dezincification process, i.e. the preferential dissolution of zinc leaving a porous residue rich in copper.[9] Conversely, the knowledge about passivity breakdown and pitting corrosion failures of this material in aggressive anion containing solutions,[10,11] is rather limited.

Manuscript received 19 April 1994; in amended form 24 June 1994.

This series of papers is devoted to a comparative electrochemical investigation of the pitting corrosion of α-, β-, and $(\alpha + \beta)$-brass in borate–boric acid buffer (pH 9) with different NaCl concentrations ($0.01\ M < c_{NaCl} < 0.5\ M$). The first part of this work shows that pitting corrosion of brass occurs at potentials slightly more negative than the breakdown potential of polycrystalline Cu, and at markedly more positive potentials than that of polycrystalline Zn. The lower corrosion resistance of these alloys in comparison to Cu is attributed to the passive layer structure consisting of a complex $ZnO \cdot xH_2O/Cu_2O$–CuO layer which is less protective towards the attack of Cl^- ions than the Cu_2O–CuO passive layer produced on Cu. Accordingly, the resistance of brass to pitting increases from $(\alpha + \beta)$- and β-brass to α-brass, the latter approaching the pitting corrosion behaviour of Cu. The greater resistance of brasses to pitting corrosion as compared to Zn is due to the formation of an outer Cu rich layer resulting from brass dezincification as $ZnO \cdot xH_2O$ and soluble Zn^{2+} species are produced.

EXPERIMENTAL METHOD

Working electrodes (specimens) were made from α, β and $(\alpha + \beta)$ brass rods, with the following chemical composition (wt%); α-brass, 71.719 Cu, 28.228 Zn, 0.011 C, 0.008 Al, 0.031 Sn, 0.001 As; β-brass, 52.460 Cu, 47.490 Zn, 0.026 C, 0.005 Al, 0.023 Sn, As and Si < 0.001; and $(\alpha + \beta)$-brass, 60.764 Cu, 38.814 Zn, 0.002 C, 0.010 Al, 0.068 Sn, 0.081 Si, 0.143 Mn, < 0.001 As.

Brass bars were made by melting and casting known amounts of Cu and Zn. The composition of the starting metals was Cu 99.999% and Zn 99.999%. Drawn brass bars 0.6 cm in dia were machined to obtain cylindrical specimens 0.3 cm in diameter. The base of the brass cylinder was used as the working electrode, which was mounted as a horizontal disc electrode in contact with a hanging electrolyte column.[12] The working electrode was wet polished using different grain size emery papers and finishing with 1 μm grit alumina paste. Then, each specimen was successively rinsed in ultrasonics with distilled acetone, twice distilled water, and dried in air at room temperature. Finally, specimens were lodged under low Ar pressure in a Pyrex tubing, and thermally treated at 150°C for 2 h to eliminate residual mechanical stresses, and to improve the surface homogeneity. This pretreatment assured a good reproducibility of results.

The alloy microstructure was studied by etching the specimens in acid $FeCl_3$ media.[13] Electrochemical runs were made in borate–boric acid buffer ($0.075\ M\ Na_2B_4O_7 + 0.15\ M\ H_3BO_3$, pH 9) and in the same buffer solution containing x M NaCl ($0.01 < x < 0.5$), at 25°C, using a conventional three-electrode Pyrex glass cell. The potential of each specimen was measured against a saturated calomel electrode (SCE) provided with a Luggin–Haber capillary tip. A platinum wire was used as counterelectrode.

Conventional triangular potential sweep voltammograms at the potential sweep rate $v = 0.02\ V\ s^{-1}$, and anodic polarization curves at $v = 2 \times 10^{-4}\ V\ s^{-1}$ from the potential $E = -0.6$ V upwards were recorded.

EXPERIMENTAL RESULTS

Voltametric data on borate–boric acid buffer, pH 9

Voltammetry was run in the borate–boric acid buffer with Zn, Cu, α-, β- and $(\alpha + \beta)$-brass specimens at $v = 0.02\ V\ s^{-1}$ between $E_{sc} = -1.4$ V and $E_{sa} = 1.0$ V to compare the potential range of the different electrochemical reactions.

Polycrystalline Zn electrodes. The first voltammogram run with a Zn specimen (Fig. 1a) shows the formation of $ZnO \cdot xH_2O$ at ca. −1.10 V (peak AI), and probably, a certain amount of soluble Zn^{2+} species.[14] As the potential is shifted positively, hump AII is detected at −0.8 V. The pseudo-limiting current recorded from $E = -0.8$ V upwards is related to the simultaneous growth of a passive layer and

Zn electrodissolution through the passive layer. The reverse potential scan shows that the electroreduction of the layer commences at $E = -0.9$ V and exhibits a broad cathodic wave CII followed by a well defined cathodic peak at $E = -1.20$ V (peak CI) which is related to the electroreduction of the $Zn(OH)_2$ formed at AI. The wave CII is related to the anodic hump AII, whereas peak CI is related to the anodic peak AI.

Voltammetric runs in which E_{sa} is gradually increased positively show that the amount of charge related to $ZnO \cdot xH_2O$ electroreduction continues increasing at least up to 1.0 V. Seemingly, the electroreduction of the $ZnO \cdot xH_2O$ layer requires a greater negative potential as the amount of anodic oxide layer is increased. This fact suggests that a change in the structure and/or composition of the anodic layer takes place as E_{sa} is shifted positively. These results agree with those previously reported by Mishima *et al.*[14]

Polycrystalline Cu electrodes. The first voltammogram of a Cu specimen in the borate–boric acid buffer run from $E_{sc} = -1.4$ V to $E_{sa} = 1.0$ V (Fig. 1b) shows the appearance of a small anodic current at $E = -0.45$ V, which corresponds to the formation of Cu(OH) surface species.[15] When $E > -0.25$ V, Cu_2O growth begins.[15,16] As already reported, Cu_2O and $CuO \cdot xH_2O$ formation are related to broad beak AIII.[15] Furthermore, for $E > 0.20$ V, a potential independent current range in which the growth of a Cu_2O inner and $CuO \cdot xH_2O$ outer complex passive layer, and Cu electrodissolution through the passive layer are observed.[15] For $E > 0.9$ V, the oxygen evolution reaction takes place. The electroreduction voltammogram shows a cathodic current peak ($CIII_a$) at $E = -0.30$ V, related to the CuO to Cu_2O electroreduction, followed by another broad peak ($CIII_b$) at $E = -0.65$ V which involves the electroreduction of Cu_2O to Cu.[16] Finally, for $E < -0.8$ V, the electroreduction of residual Cu^+ species takes place simultaneously with the hydrogen evolution reaction. The subsequent potential cycling indicates that the oxide layer electroreduction at E_{sc} is still incomplete as the anodic current peak height slightly decreases. All these voltammetric features coincide with those earlier reported for Cu in the same environment.[15,16]

Polycrystalline brass electrodes. The voltammograms run with α-brass specimens (Fig. 1c) exhibit peaks AI and AII which correspond mainly to the formation of $ZnO \cdot xH_2O$ and certain amount of soluble Zn^{2+} species, as for polycrystalline Zn. Thus, cathodic peaks at $E = -0.9$ V (CII) and $E = -1.2$ V (CI) can be assigned to the electroreduction of ZnO to Zn. Peak AIII, which corresponds to the Cu_2O–CuO electroformation, is broad and somewhat ill-defined for brass. However, the electroreduction of CuO oxide to Cu_2O and the electroreduction of Cu_2O to Cu originate two well defined cathodic peaks located at -0.3 V ($CIII_a$) and -0.65 V ($CIII_b$), respectively. These reactions occur in the -0.5 V to -0.8 V range, and extend to further negative potentials, partially overlapping the electroreduction of ZnO species (peak AII).

For β-brass (Fig. 1d) and $(\alpha + \beta)$-brass (Fig. 1e) the voltammograms are comparable to those recorded for α-brass. These voltammograms indicate that the passive layer for all brass is made of Cu oxides and $Zn(OH)_2$.

For all brass, as well as Cu and Zn specimens, solution stirring produces no marked changes in the potential ranges of the pairs of peaks AI/CI, AII/CII, AIII/CIII. Therefore, these peaks can be assigned to metal electro-oxidation yielding

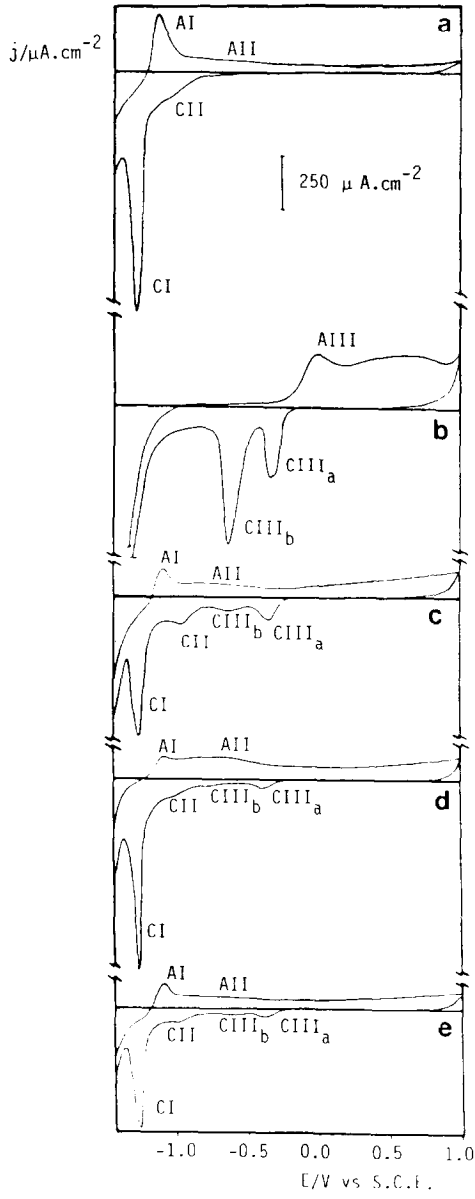

Fig. 1. First current density (j) vs potential (E) profiles at 0.02 V s^{-1} (a–e) and j vs E profiles with increasing E_{sa} run at 0.1 V s^{-1} (f–h). (a) Zn; (b) Cu; (c) and (f), α-brass; (d) and (g), β-brass; (e) and (h), ($\alpha + \beta$)-brass. Borate–boric acid buffer at 25°C.

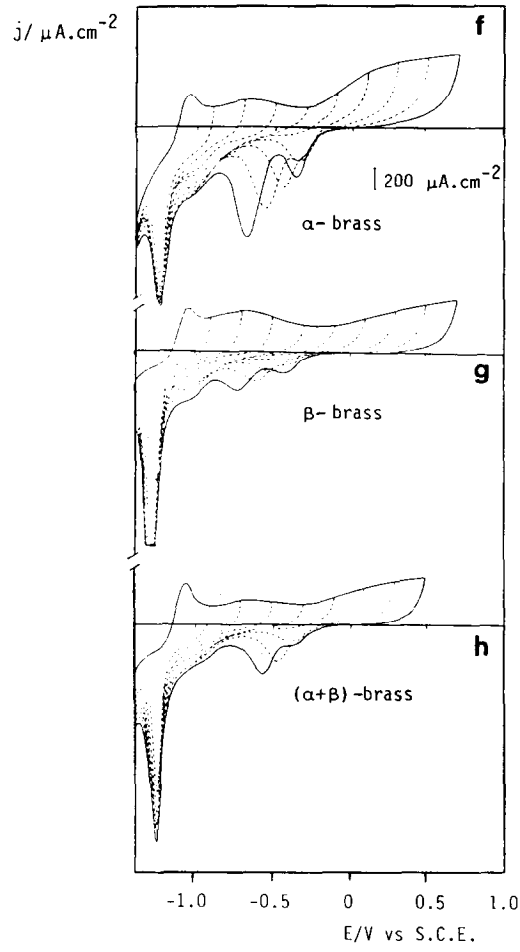

Fig. 1. *Continued.*

oxide species rather than to the electroformation of soluble species, although small amounts of soluble species could be detected by using the rotating ring-disc electrode technique.[15]

Voltammetric runs at $v = 0.10$ V s^{-1} for the brass electrodes in which E_{sa} is gradually and positively increased (Fig. 1f–h) show that the amount of charge related to $ZnO \cdot xH_2O$ electroreduction increases in the order α-brass $<$ $(\alpha + \beta)$-brass $<$ β-brass as expected from bulk alloy compositions. The contribution of Cu_2O and $CuO \cdot xH_2O$ to the passive layer composition appears only when E_{sa} exceeds -0.25 and 0.25 V, respectively, as determined from peaks $CIII_b$ and $CIII_a$. Note that the potential required to form a certain amount of reducible CuO species is more positive for brass than for polycrystalline Cu.[15] The amount of Cu oxides in the passive layer increases in the order β-brass $<$ $(\alpha + \beta)$-brass $<$ α-brass following the increase in the Cu content of these alloys. For all brass the amount of ZnO and Cu_2O–CuO continues increasing at least up to 0.7 V. Seemingly, the electroreduction of these oxides requires a greater negative potential as the amount of oxide is increased. Again, this is an indication that a change in the structure and/or

composition of the anodic layer takes place as Esa is moved positively as reported for polycrystalline Cu and Zn in the borate–boric acid buffer.[14,15]

Voltammetric data on NaCl-containing borate–boric acid buffer

Voltammograms of Cu, Zn, α-, β- and ($\alpha + \beta$) brass were also run in x M NaCl + borate buffer ($10-3 \leq x \leq 10-1$) under the same conditions described for voltammetric data on borate–boric acid buffer, pH 9.

Voltammograms for Cu and brass specimens (Figs 2–4, b–e) for $10^{-3} \leq x \leq 10^{-1}$ are qualitatively comparable to those obtained in the plain buffer. However, the anodic current in the passive region increases with c_{NaCl} a fact which suggests an increase in the amount of Zn^{2+}, Cu^{+}, and Cu^{2+} soluble species with c_{NaCl}. On the other hand, for $x \geq 0.1$ M a substantial increase in the anodic current occurs when $E > E_b$, the breakdown potential value.[15,17] The reverse scan involves a current loop related to the nucleation and growth of pits.[15] In this case, the anodic to cathodic current switching takes place at $E_r \cong 0.05$ V, where E_r denotes the repassivation potential. The cathodic current is considerably enhanced due to the electroreduction of those soluble species produced during pitting.

Voltammograms run for Zn and $10^{-3} \leq x \leq 10^{-1}$ (Figs 2–4, a) are similar to those described for the plain buffer, although the anodic current in the passive range increases with c_{NaCl}. For $x \geq 10^{-3}$, the typical localized corrosion current loop appears when $E > E_b$. The anodic to cathodic current switching takes place at $E_r = -0.20$ V for $x = 10^{-3}$ and at $E_r = -0.9$ V for $x = 10^{-2}$ and $x = 10^{-1}$. Therefore, low c_{NaCl} values favour the localized corrosion of Zn, in contrast to Cu and brass which require $x \geq 0.05$.

Breakdown potential measurements

Values of E_b for the different brasses were determined from anodic polarization curves recorded from -0.6 V upwards at $v = 2 \times 10^{-4}$ V s^{-1} in the NaCl-containing borate–boric acid buffer ($5 \times 10^{-2} \leq x \leq 0.5$) (Fig. 5). The value of E_b was defined as the highest positive potential involving an anodic current in the passivity range. As observed for other systems,[18] E_b values are usually distributed over a rather broad potential range. In this case, a parameter such as $P_{n\geq1}$, the probability to form at least one stable pit, can be used. $P_{n\geq1}$ is defined as:[18]

$$P_{n\geq1}(E) = N(E)/N_t, \tag{1}$$

where N is the number of specimens that develop pitting at a given potential E, and N_t is the total number of specimens. The accumulative $P_{n\geq1}$ vs E plots derived from anodic polarization curves for α-, β- and ($\alpha + \beta$)-brass in 0.5 M NaCl (Fig. 6a) indicate that the pitting potential range is relatively broad, and shifts positively following the order ($\alpha + \beta$)-brass $\cong$ β-brass $<$ α-brass. Similar plots resulting from the $1 \times 10^{-2} \leq x \leq 0.5$ range indicate that the pitting potential range for each type of brass shifts positively as x is decreased (Fig. 6b).

$\langle E_b \rangle$, the mean value of E_b, defined as the potential value for $P_{n\geq1} = 50\%$, depends on log c_{NaCl} as seen in Fig. 7 for the three types of brass. $\langle E_b \rangle$ shifts negatively as c_{NaCl} is increased. The $\langle E_b \rangle$ vs log c_{NaCl} plots result in straight lines with slopes -0.36 V decade^{-1}, -0.43 V decade^{-1} and -0.40 V decade^{-1} for α-, β- and ($\alpha + \beta$)-brass, respectively (Fig. 7), although these lines shift in the negative potential direction as the Zn content in brass increases. The $\langle E_b \rangle$ vs log c_{NaCl} plots for

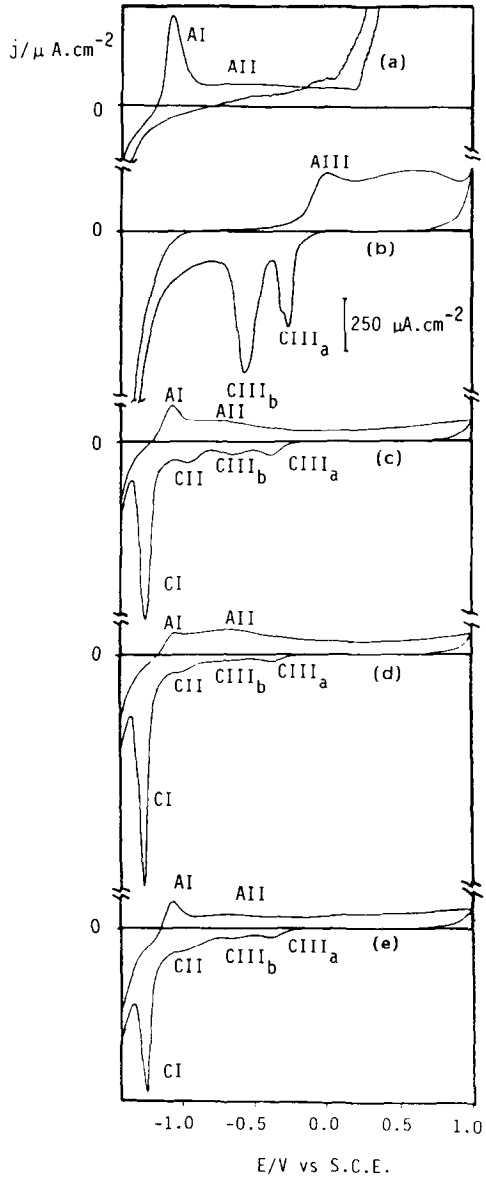

Fig. 2. First j vs E profiles run at 0.02 V s^{-1}. (a) Zn; (b) Cu; (c) α-brass; (d) β-brass; (e) $(\alpha + \beta)$-brass. Borate–boric acid buffer $+10^{-3}$ M NaCl at 25°C.

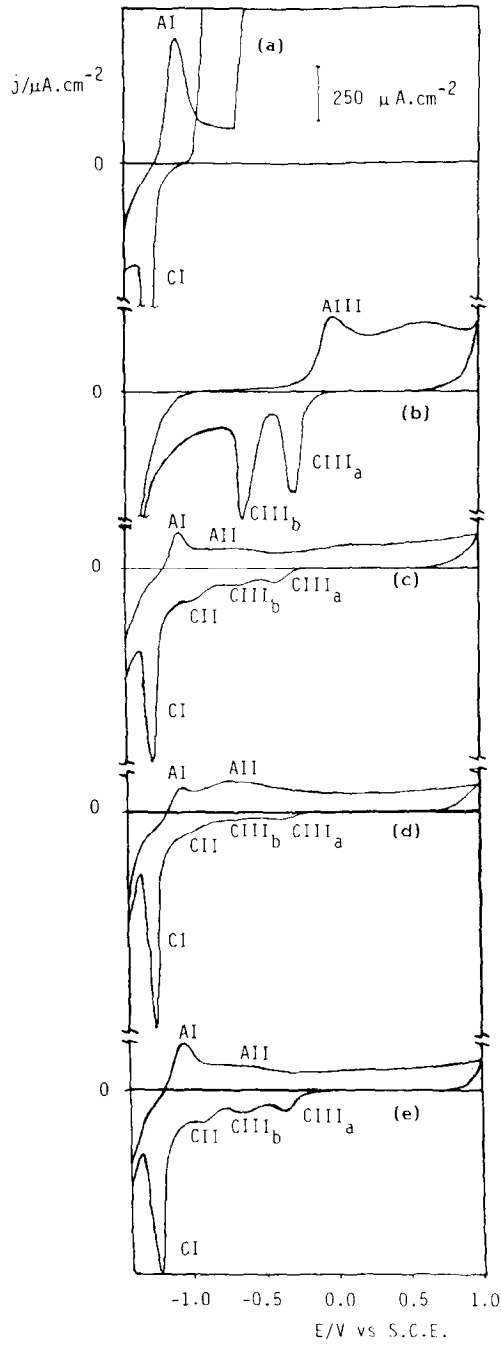

Fig. 3. First j vs E profiles run at 0.02 V s^{-1}. (a) Zn; (b) Cu; (c) α-brass; (d) β-brass; (e) ($\alpha + \beta$)-brass. Borate–boric acid buffer $+10^{-2}$ M NaCl at 25°C.

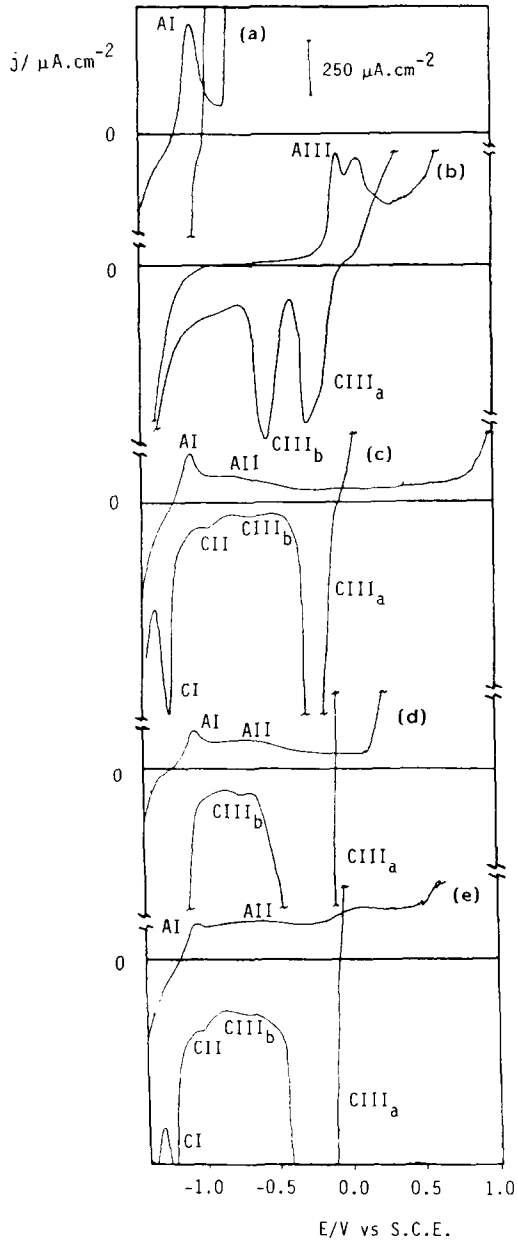

Fig. 4. First j vs E profiles run at 0.02 V s^{-1}. (a) Zn; (b) Cu; (c) α-brass; (d) β-brass; (e) $(\alpha + \beta)$-brass. Borate–boric acid buffer $+10^{-1}$ M NaCl at 25°C.

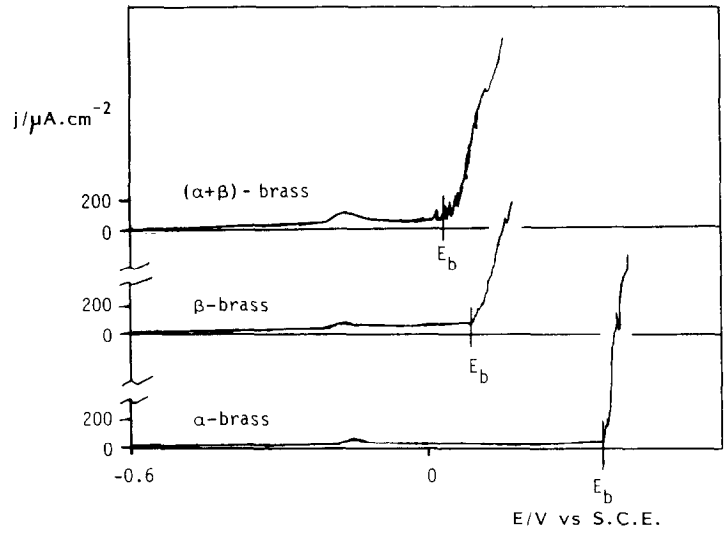

Fig. 5. Typical anodic polarization curves for the three types of brass run at $v = 2 \times 10^{-4}$ V s^{-1}. Borate–boric acid buffer +0.5 M NaCl at 25°C.

brass bear a closer resemblance to the same plot for polycrystalline Cu than to that of polycrystalline Zn. Besides, the slopes of the straight lines are very similar to that found for Cu.[15]

These results indicate that the pitting corrosion resistance of brasses in the tested solutions increases in the order $(\alpha + \beta)$-brass $\cong$ β-brass $<$ α-brass. $\langle E_b \rangle$ values for brass are always hundreds of mV more positive than that for polycrystalline Zn (Fig. 7).

Induction time measurements

Values of t_i, the induction time for pit initiation, were obtained for the different brasses in the borate–boric acid buffer + 0.5 M NaCl from current transients run at a constant potential (0 V $< E_s <$ 0.6 V) (Fig. 8a). When $E_s < E_b$ the anodic current decreases continuously due to the passive layer growth and finally, it reaches a constant value related to the corrosion current through the passive layer (Fig. 8a, dashed line). On the other hand, for $E_s > E_b$, the anodic current first decreases and then increases due to pit growth (Fig. 8a, solid line). The time related to the current minimum has been taken as the induction time for pit initiation.[15] For all brass the value of t_i decreases sharply as E_s is moved positively to attain a constant and small value (Fig. 8b). At constant E_s, values of t_i are larger for α-brass than for β- and $(\alpha + \beta)$-brass.

Microscopy imaging

Micrographs of the microstructure of alloys. Micrographs of the α-, β- and $(\alpha + \beta)$ brass specimens after etching in acid $FeCl_3$ are basically different. Thus, α-brass shows the typical structure of crystallographic grains which exhibits a very mild corrosion as seen by the permanence of polishing lines after etching. Likewise, β-brass also shows a crystallographic structure consisting of large grains which becomes

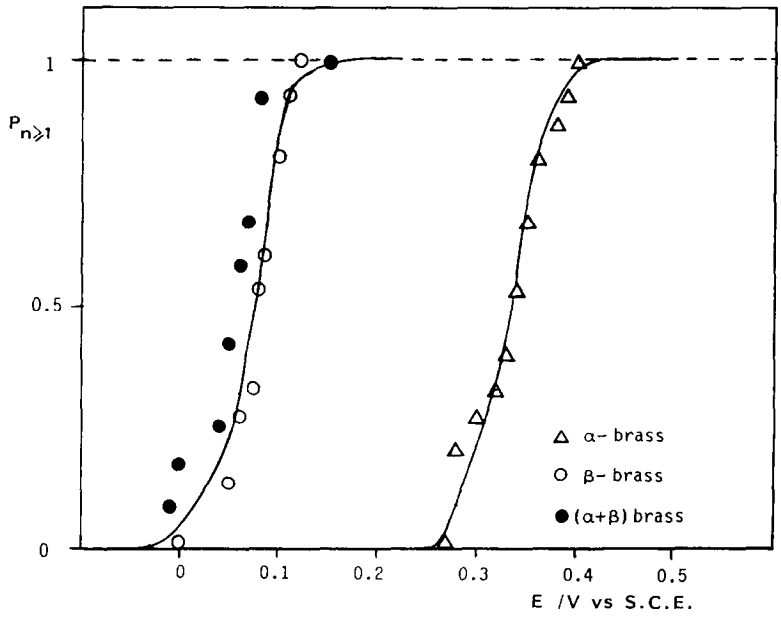

(a)

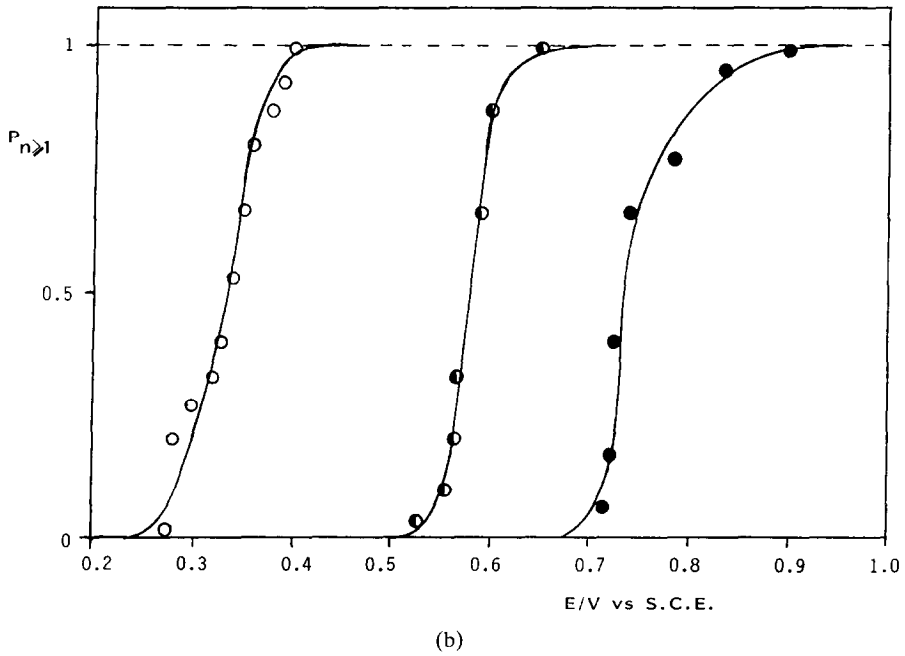

(b)

Fig. 6. (a) $P_{n\geqslant 1}$ vs E plots for (△) α-brass; (○) β-brass and (●) $(\alpha + \beta)$-brass. Borate–boric acid buffer +0.5 M NaCl; (b) $P_{n\geqslant 1}$ vs E plots for $(\alpha + \beta)$-brass. Borate–boric buffer $+x$ M NaCl. (●) $x = 0.05$; (○) $x = 0.1$; (◐) $x = 0.5$ at 25°C.

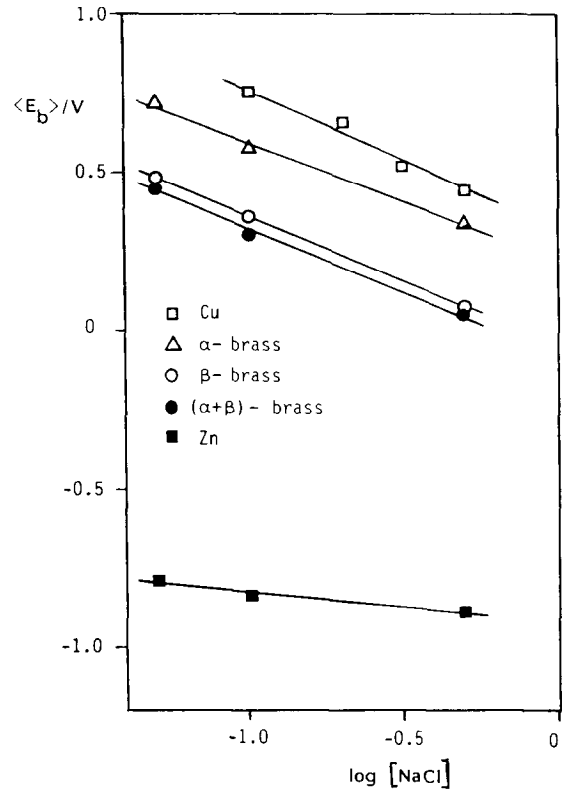

Fig. 7. $\langle E_b \rangle$ vs log c_{NaCl} plots for (△) α-brass; (•) β-brass; (●) ($\alpha + \beta$)-brass; (□) Cu; (■) Zn. Borate–boric acid buffer $+x$ M NaCl at 25°C.

more prone to corrosion. Finally, ($\alpha + \beta$)-brass presents a rather deep general attack which leads to an island structure resulting from the preferential attack of the β-phase.

Micrographs in the passivity range. Micrographs of ($\alpha + \beta$)-, α-, and β-brass after anodization at O V ($E_s < E_b$) for 1 min in borate–boric acid buffer + 0.5 M NaCl, reveal only scratches from the mechanical polishing. No other corrosion features can be observed on these specimens.

Micrographs in the pitting corrosion range. SEM micrographs of α-brass specimens resulting after anodization at $E_s = 0.4$ ($E_s > E_b$) for 40 s in borate–boric acid buffer + 0.5 M NaCl (Fig. 9a) show a few large and shallow pits, some small pits and free corrosion areas. Conversely, SEM micrographs of β-brass specimens anodized as indicated above (Fig. 9b) show large and deep pits and also a large number of small pits which overlaps leading to a non-uniform corrosion. Finally, SEM micrographs of ($\alpha + \beta$)-brass specimens under the same experimental conditions show a preferential non-uniform attack at the β phase (Fig. 9c) resulting from the overlap of a large number of pits. On the other hand, isolated pits can be detected in the α-phase regions.

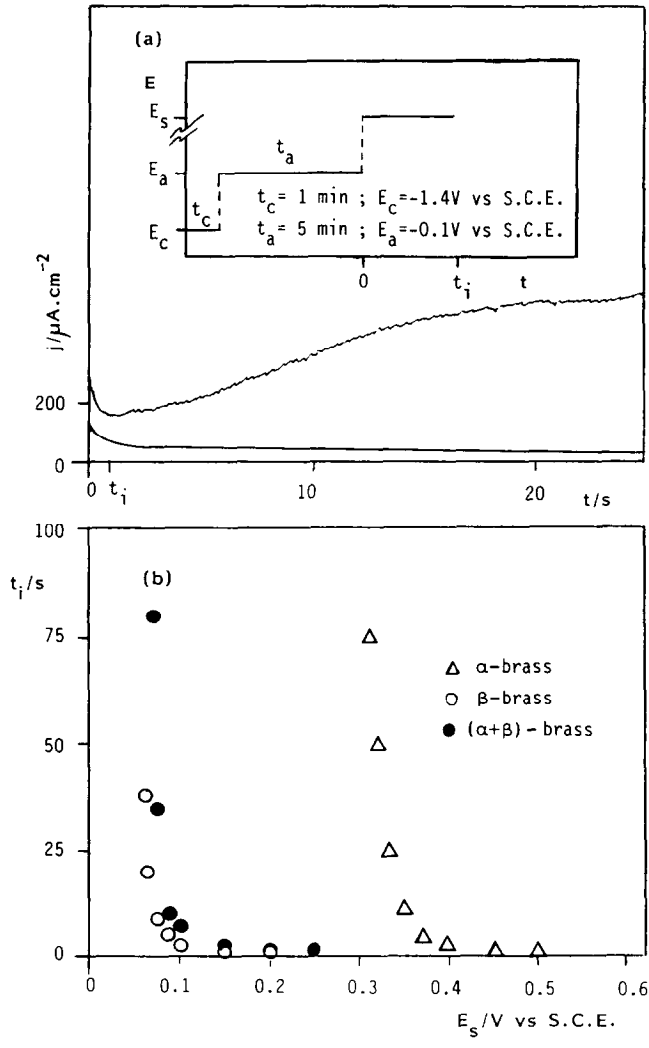

Fig. 8. (a) Typical current transients at constant potential (E_s) for $E_s < E_b$ (dashed line) and for $E_s > E_b$ (solid line); (b) t_i vs E_s plots for (△) α-brass, (○) β-brass and (●) ($\alpha + \beta$)-brass. Borate–boric acid buffer +0.5 M NaCl at 25°C.

The accumulation of corrosion products at the border and bottom of pits were observed for all brass anodized in the pitting corrosion potential range.

X-ray diffractometry

A green precipitate is formed during pitting in the borate–boric acid buffer containing 0.5 M NaCl for all brass. X-ray diffractometry data (Fig. 10) show that the precipitate corresponds to $(Cu,Zn)(OH)_3Cl$. It should be noted that the formation of this compound has been identified as a corrosion product from brass heat exchangers in contact with sea water.[11]

DISCUSSION

The corrosion and passivation of Cu and Zn, the brass alloy components, have been extensively studied over a wide range of experimental conditions. Passivation of Cu in aqueous alkaline solutions[15,16,19,20] implies the initial formation of a Cu_2O monolayer, and as E is positively shifted, the formation of an inner Cu_2O and an outer CuO hydrated layers begins. The electrochemical behaviour of these passive layers depends considerably on the solution composition and temperature.[3] In the presence of aggressive anions such as Cl^-,[15] Br^-[19] and SO_4^{2-} ions[21] localized corrosion of Cu occurs when $E > E_b$.[15,19,20] The pitting corrosion of Cu in borate–boric acid buffer containing NaCl, covering the 0–70°C temperature range, has been reported.[20] On the other hand, the passivation of Zn in alkaline solutions involves the electroformation of a $ZnO \cdot xH_2O$ layer.[14] In the presence of aggressive anions such as halide ions, passivity breakdown and pitting corrosion of Zn occurs at E values more negative than those found for Cu under similar conditions.

Voltammetric data presented in this work reveal that the passive layer on brass involves at least two stages. The first stage occurs at $E < -0.25$ V and it results in the formation of a $ZnO \cdot xH_2O$ layer. This process can be represented by the following equation:

$$[Zn/Cu]\ (Zn/Cu) + x\ H_2O = [Zn/Cu]\ (Cu \cdot ZnO \cdot (x - 1)\ H_2O) + 2\ H^+ + 2e^- \quad (2)$$

where the brackets and parenthesis denote bulk alloy and surface species, respectively. Note that this process also leads to an alloy/metal oxide interface richer in Cu.

The second stage occurs when $E > -0.25$ V, and it involves the electroformation of a Cu_2O layer in the potential range of peak A(III). This process can be expressed as:

$$[Zn/Cu]\ (Cu \cdot ZnO \cdot (x - 1)\ H_2O) + H_2O = [Zn/Cu]\ (Cu_2O \cdot ZnO \cdot (x - 1)\ H_2O) + 2\ H^+ + 2e^- \quad (3)$$

Thus, according to equations (2) and (3) the anodic layer on brasses implies a composed layer with Cu_2O and ZnO constituents.

Finally, for $E > 0.2$ V, the electroformation of CuO in the passive layer takes place as detected in the voltammograms.

Voltammetric data for brass in 0.5 M NaCl-borate–boric acid buffer, indicate that the anodic layer as described above is modified by the presence of Cl^- ions. Thus, the current associated with both the passive region and peak CI increases with c_{NaCl} probably because of an increase in the amount of soluble ionic species. This process can be explained through the following equation:

$$n(Cu_2O \cdot ZnO \cdot (x - 1)\ H_2O) + pCl^- = (n - 2p)\ (Cu_2O \cdot ZnO \cdot (x - 1)\ H_2O) + p/2\ Cl_2Cu^- + pCl_4Zn^{2-} \quad (4)$$

According to this equation an enhanced flux of cations and/or vacancies through the anodic layer occurs due to the presence of Cl^- ions at the passive layer/solution interface. This type of process and the intrinsic thickness and composition inhom-

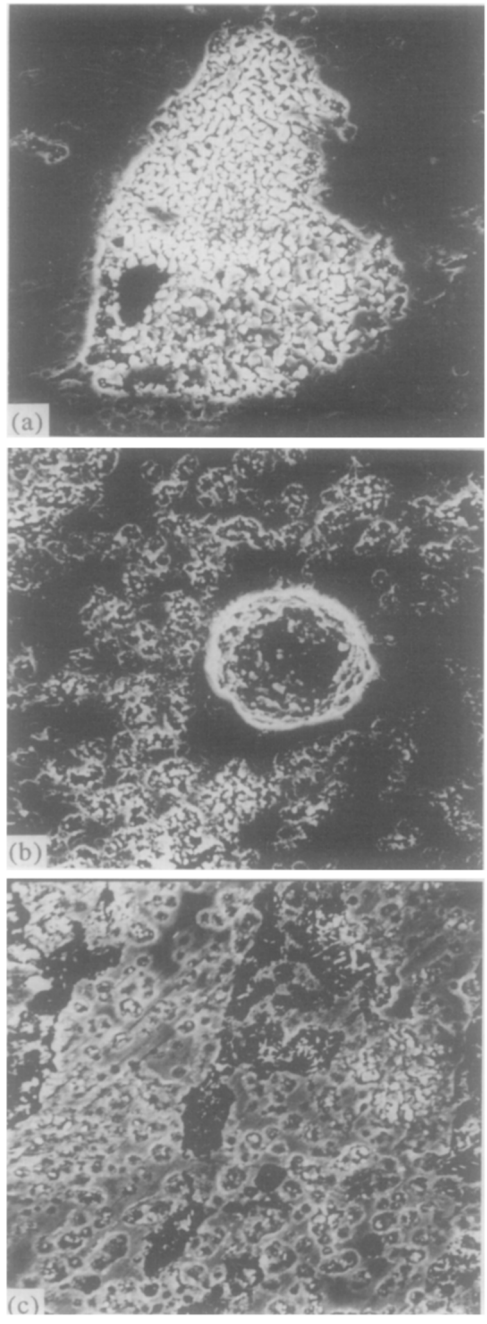

Fig. 9. SEM micrographs after brass anodization at $E_s = 0.4$ V ($E_s > E_b$) for $t = 40$ s in borate–boric acid buffer + 0.5 M NaCl; (a) α-brass (1500×), (b) β-brass (1500×) and (c) ($\alpha + \beta$)-brass (1500×).

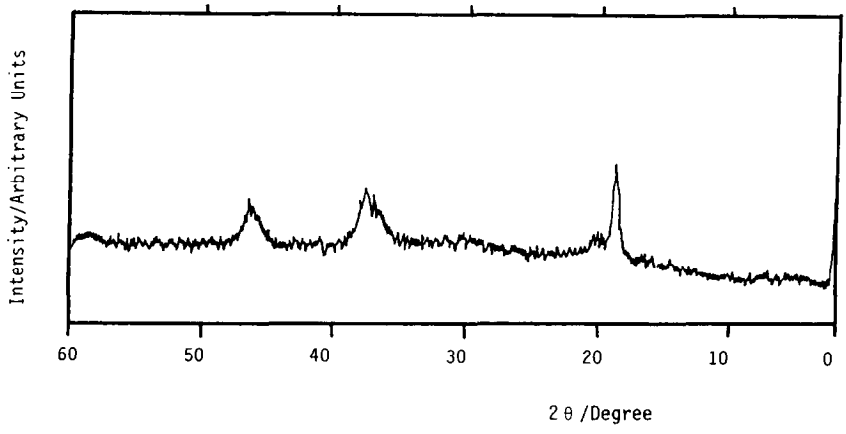

Fig. 10. X-ray diffractrogram of the corrosion products formed during pitting of ($\alpha + \beta$)-brass in borate–boric acid buffer +0.5 M NaCl.

ogeneity of the passive layer can explain the breakdown of passivity and the pitting corrosion of brass.

The differences observed for the localized corrosion resistance of Cu and brass can be, in principle, attributed to differences in the passive layer specific composition and structure. At a constant temperature and c_{NaCl}, values of $\langle E_b \rangle$ for the three types of brass are more negative than that of polycrystalline Cu.[15] However, for β- and ($\alpha + \beta$)-brass values of $\langle E_b \rangle$ are rather different from that of Cu, in contrast to the value of $\langle E_b \rangle$ for α-brass (Fig. 7). Thus, it can be argued that the ZnO/Cu_2O–CuO duplex structure of brass is less resistant to Cl^- ion attack than the Cu_2O/CuO layer formed on Cu, presumably due to the heterogeneity of the ZnO/Cu_2O–CuO layer. On the other hand, the ZnO/Cu_2O–CuO layer on brass becomes more resistant to passivity breakdown than the ZnO layer formed on Zn under the same conditions (Fig. 7). Accordingly, the localized corrosion resistance of brass should increase as the content of ZnO in the passive layer decreases as concluded from experiments. However, this approach to the pitting corrosion of brasses exclusively based on the passive layer properties fails to explain the resistance of brasses to localized corrosion at potential values where pitting corrosion of Zn occurs.

As shown in Fig. 7, the pitting corrosion of polycrystalline Zn in the 0.01 M $\leq c_{NaCl} \leq$ 0.5 M range occurs at potentials more negative than -0.5 V, i.e. in a potential range where the metal surface is covered by a ZnO·xH_2O layer. As Cu electro-oxidation to form a CuOH adsorbed monolayer occurs at potentials more positive than -0.5 V,[15] it should be expected that a brass surface be covered only by a ZnO·xH_2O layer in this potential range. Therefore, the increased localized corrosion resistance of brass with respect to polycrystalline Zn cannot be explained in terms of simple passive layer properties of the pure alloy components. It is possible that the selective Zn dissolution induces Cu oxide formation at potentials lower than those observed for polycrystalline Cu as reported for Cu–5Al–5Sn.[17] The voltammetric results obtained in this work show no evidence of Cu oxide formation as current peaks $CIII_a$ and $CIII_b$ are absent when E_{sa} is set at $E < -0.5$ V. In terms of passive film properties no differences would be expected for $\langle E_b \rangle$ values of Zn and

brass, opposite to experimental results showing that $\langle E_b \rangle$ values for brass are $\cong$ 0.7–1.0 V more positive than that corresponding to polycrystalline Zn. This would mean that some additional characteristics of the passive layer determine the localized corrosion resistance of brass.

A more reasonable explanation can be given by considering the actual composition of the metal surface remaining under the $ZnO \cdot xH_2O$ layer. The selective dissolution of brass at $E < -0.5$ V yielding $ZnO \cdot xH_2O$ and soluble Zn^{2+} species, results in a thin Cu rich surface layer at the alloy/oxide layer interface as detected by XPS and AES.[22] Passivity breakdown at the $ZnO \cdot xH_2O$ layer exposes thin Cu rich alloy domains which are immune to corrosion in this potential range (Figs 2–4). As the case of de-alloying processes below the critical potential value, the thin layer of the more noble metal hinders corrosion.

Pitting of brass occurs in the potential region where Cu^+ and Cu^{2+} species are detected.[15] Thus, reactions within the pit can be represented as follows:

$$[Zn/Cu]\ (Zn/Cu) + 6\ Cl^- = Cl_2Cu^- + Cl_4Zn^{-2} + 3\ e^-, \quad (5)$$

and

$$[Zn/Cu]\ (Zn/Cu) + 5\ Cl^- = CuCl + Cl_4Zn^{-2} + 3\ e^-, \quad (6)$$

$$[Zn/Cu]\ (Zn/Cu) + 4\ Cl^- + = Cl_4Zn^{-2} + ClCu^+ + H^+ + 4e^-, \quad (7)$$

followed by the precipitation of $(Cu,Zn)\ (OH)_3Cl$ through:

$$Cl_4Zn^{-2} + ClCu^+ + 3\ H_2O = (Cu,Zn)\ (OH)_3Cl + 3\ H^+ + 4\ Cl^-. \quad (8)$$

Reaction (6) takes into account the presence of CuCl at the pit bottom as observed during Cu pitting in Cl^- ion-containing solutions.[11] Reaction (8) explains the formation of the green $(Cu,Zn)(OH)_3Cl$ precipitate identified in this work during brass pitting in borate–boric acid buffer containing ClNa anions. The same compound has been reported for pitting of admiralty brass heat exchangers in sea water.[11]

CONCLUSIONS

The pitting corrosion of brass in NaCl-borate–boric acid buffer, pH 9, and at 25°C, occurs at potential values slightly more negative than the breakdown potential of Cu, and markedly positive with respect to that of Zn. The lower pitting corrosion resistance of brass as compared to Cu is due to the presence of a complex $ZnO \cdot xH_2O/Cu_2O$–CuO layer which is less protective towards Cl^--ion attack than the Cu_2O–CuO layer formed on Cu. Accordingly, the pitting resistance increases from the $(\alpha+\beta)$- and β-brasses to α-brass, the latter approaching the Cu behaviour. The increase in resistance of brass to pitting corrosion with respect to Zn is due to the formation of a Cu-rich layer at the alloy/oxide layer interface which is immune to corrosion at negative potentials where the pitting corrosion of Zn takes place in NaCl containing solutions. The Cu rich layer arises from the brass dezincification during $ZnO \cdot xH_2O$ and soluble Zn^{2+} species electroformation.

Acknowledgements—Authors thank UNELCO S.A. (Unión Eléctrica de Canarias S.A.) and Dirección General de Investigación Científica y Técnica (DGICYT) (Spain) for the financial support of this work. AJA and RCS also thank CONICET (Argentina).

REFERENCES

1. H. W. Pickering and C. Wagner, *J. electrochem. Soc.* **114**, 698 (1967).
2. R. C. Newman, T. Shahrabi and K. Sieradzki, *Corros. Sci.* **28**, 873 (1988).
3. J. C. Scully, *Met. Sci.* **12**, 290 (1978), and references therein.
4. D. Hardie and K. Ebtehaj, *Br. Corros. J.* **22**, 202 (1987).
5. H. W. Pickering, *Corros. Sci.* **23**, 1107 (1983).
6. T. P. Moffat, R. F. Fan and A. J. Bard, *J. electrochem. Soc.* **138**, 3224 (1991).
7. K. Trethewey and J. Chamberlain, *Corrosion*, Longman, Essex, (1988), and references therein.
8. D. R. Askeland, *The Science and Engineering of Materials*, PWS–Kent Publishing Company, Boston (1989).
9. C. M. Rangel and A. L. De Sá, *Progress in The Understanding and Prevention of Corrosion* (eds J. M. Costa and A. D. Mercer), p. 1453. The Institute of Materials, London (1993).
10. A. G. Gad-Allah, M. M. Abou-Romia, M. W. Badawy and H. H. Rehan, *J. appl. Electrochem.* **21**, 829 (1991).
11. Z. Szklarska-Smialowska, *Corrosion* **46**, 85 (1990).
12. C. I. Elsner, P. L. Schilardi and S. L. Marchiano, *J. appl. Electrochem.* **23**, 1181 (1993).
13. ASTM Standard, Part I-B (1946).
14. H. Mishima, A. B. Lopez de Mishima, E. Santos, C. P. De Pauli, K. Aumi and N. Sato, *Electrochim. Acta* **36**, 1491 (1991).
15. M. R. G. de Chialvo, R. C. Salvarezza, D. Vasquez Moll and A. J. Arvia, *Electrochim. Acta.* **30**, 1501 (1985).
16. H. H. Strehblow and B. Titze, *Electrochim. Acta* **25**, 339 (1980).
17. T. Suter, E. M. Moser and H. Böhni, *Corros. Sci.* **34**, 1111 (1993).
18. R. C. Salvarezza, N. De Cristofaro, C. Pallotta and A. J. Arvia, *Electrochim. Acta* **32**, 1049 (1987).
19. M. R. G. de Chialvo, M. F. L. de Mele, R. C. Salvarezza and A. J. Arvia, *Corros. Sci.* **28**, 121 (1988).
20. M. G. Figueroa, R. C. Salvarezza and A. J. Arvia, *Electrochim. Acta* **31**, 665 (1986).
21. R. Souto, S. González, R. C. Salvarezza and A. J. Arvia, *Electrochim. Acta* (in press).
22. J. Morales, P. Esparza, G. T. Fernández, S. González, J. E. García, J. Cáceres, R. C. Salvarezza and A. J. Arvia, *Corrosion Sci.* **37**, 231 (1995).